

Topological characterization of non-Hermitian multiband systems using Majorana's Stellar Representation

Wei Xin Teo,¹ Linhu Li,^{1,*} Xizheng Zhang,¹ and Jiangbin Gong^{1,†}

¹*National University of Singapore, Department of Physics*

(Dated: May 20, 2020)

For topological characterization of non-Hermitian multiband systems, Majorana's stellar representation (MSR) is applied to 1D multiband models consisting of asymmetric nearest-neighbor hopping and imaginary on-site potentials. The number of edge states isolated from the continuous bulk bands in the complex energy plane is successfully linked with a topological invariant constructed from MSR. Specifically, the number of isolated edge states can be obtained from a winding number defined for the Majorana stars, which also allows for a geometric visualization of the topology related to the isolated edge modes. A remarkable success of our approach is that our winding number characterization remains valid even in the presence of exceptional points of the continuous bulk bands, where the Hamiltonian becomes non-diagonalizable and hence conventional topological invariants such as the Zak phase and the Chern number cannot be properly defined. Furthermore, cases with the so-called non-Hermitian skin effect are also studied, showing that the bulk-boundary correspondence between our defined winding numbers and isolated edge states can be restored. Of particular interest is a four-band example with an odd number of isolated edge states, where the Zak phase approach necessarily fails upon removing the skin effect, but our MSR-based characterization works equally well. For these reasons, our study is expected to be widely useful in topological studies of non-Hermitian multiband systems, regardless of the skin effect or the presence of the exceptional points in non-Hermitian systems.

I. INTRODUCTION

Non-Hermitian Hamiltonians^{1,2} are now widely recognized to be physically relevant as effective Hamiltonians in many physical systems, such as open quantum systems³ with finite life time introduced by electron-electron or electron-phonon interactions^{4,5}, and photonic systems with gain and loss⁶⁻⁸. In particular, non-Hermitian topological phases have been one of the most intriguing research subjects during the past few years, because they possess many exotic topological phenomena beyond Hermitian systems. In non-Hermitian systems, exceptional degeneracies emerge when two or more energy levels coalesce into one, becoming identical not only in eigenenergies, but also eigenstates⁹⁻²³. Such degeneracies can form various manifolds with distinct topological structures in the Brillouin zone of systems beyond one-dimension²⁴⁻³³. The celebrated ten-fold symmetry classification has also been extended into non-Hermitian systems, and is much enriched due to the extra non-spatial symmetries of non-Hermitian matrices³⁴⁻⁴⁵. It has also been shown that the non-Hermitian skin effect (NHSE)⁴⁶, reflected by enormous accumulation of eigenmodes at system boundaries, can modify the topological bulk-boundary correspondence^{38,46-54}, and lead to other novel phenomena when interplayed with different physical effects, e.g. non-Hermitian quasicrystal⁵⁵⁻⁵⁷, hybrid skin-

topological modes and topology-controlled non-reciprocal pumping^{58,59}, emergence of a real space Fermi surface⁶⁰, and singularities in Berry curvature⁵⁴. To understand these interesting behaviors, many efforts have been made to develop new tools for characterization and geometric visualization of non-Hermitian topology, such as the generalized Brillouin zone^{46,61,62}, energy vorticity¹⁷ and the associated winding numbers^{52,63}, the singularity ring in pseudospin space³⁸, and a graphic approach of eigenstates on torus as certain parameter space⁶⁴.

To date, topology of eigenstates in non-Hermitian systems can already be geometrically visualized through various methods^{38,64-67}. However, many of them have focused on two-band systems only. It is possibly challenging but of great interest to study non-Hermitian multiband systems. In Hermitian systems, multiband topology can be analyzed with the Majorana's stellar representation (MSR)⁶⁸⁻⁷², which maps a n -band eigenstate to $n - 1$ Majorana Stars (MSs) on a Bloch sphere, each representing a different spin-1/2 state⁷²⁻⁷⁵. The distributions and motions of these MSs on a Bloch sphere are collectively connected to the Berry phase of the original n -band eigenstates, thus providing an intuitive way towards understanding the underlying topological properties. Inspired by such progresses in Hermitian multiband systems, in this work we extend the MSR approach to non-Hermitian multiband systems by defining MSs for only the right (or left) eigenstates. With explicit analysis of two-band sys-

tems and several intriguing examples of multiband systems, we find a one-to-one correspondence between the number of edge states isolated from continuous bands and a winding number defined from these MSs. Remarkably, the winding number we propose is well-defined even when different energy bands coalesce at one or more exceptional points (EPs), whereas conventional topological invariants such as the Zak phase and the Chern number are generally ill-defined in such cases. Furthermore, our method can be directly extended to systems with NHSE via a known procedure, namely, by considering the so-called non-Bloch Hamiltonian obtained by a complex deformation of the quasi-momentum of the studied system. Of particular importance, in a 4-band model with NHSE and possessing an odd number of isolated edge states, our defined winding number continues to work because it can equally predict the number of edge states in this subtle case, whereas the Zak phase necessarily fails in this situation. Putting all these results together, it can be concluded that our defined winding number provides the most potent topological invariant to date in characterizing non-Hermitian topological phases in multiband systems, where both continuous bands and isolated edge states behave very differently from Hermitian systems.

The rest of this paper is organized as follows. In Sec. II we introduce our multiband models with non-Hermiticity induced by non-reciprocal hoppings and imaginary on-site potentials. In Sec. III we briefly review the MSR of high-(pseudo)spin states, and define a winding number for the MSs of each band. Sec. IV contains the main results of this work, where we illustrate the bulk-boundary correspondence between isolated edge states and our defined winding numbers in several different scenarios with/without EPs and/or NHSE. A brief summary and discussion are given in Sec. V.

II. NON-HERMITIAN 1D MULTIBAND CHAIN MODEL

We consider a 1D lattice model with J lattice sites in a unit cell, as illustrated in Fig. 1. The corresponding tight-binding Hamiltonian is given by

$$H = \sum_n^N \sum_j^J (i\mu_j \hat{c}_{j,n}^\dagger \hat{c}_{j,n} + (t_j + \delta_j) \hat{c}_{j,n}^\dagger \hat{c}_{j+1,n} + (t_j - \delta_j) \hat{c}_{j+1,n}^\dagger \hat{c}_{j,n}), \quad (1)$$

where $\hat{c}_{j,n}$ ($\hat{c}_{j,n}^\dagger$) is the annihilation (creation) operator of a particle at the j th lattice site in the n th unit cell, and

$\hat{c}_{J+1,n} \equiv \hat{c}_{1,n+1}$. Fig. 1 presents a more specific configuration of the lattice. As indicated in Fig. 1, our model consists of $(N \times J)$ lattice sites, with non-reciprocal hopping $t_j \pm \delta_j$ (which may induce NHSE in this system), and on-site imaginary potential μ_j depicting particle gain and loss.

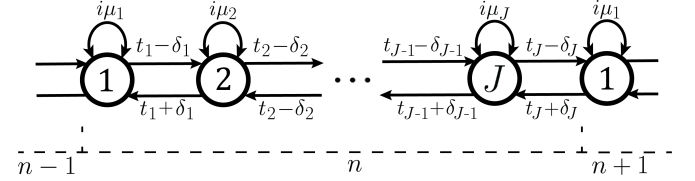


FIG. 1: A simple illustration of the non-Hermitian 1D J -band chain model. Circles indicate the lattice site and arrows indicate the hopping between the lattices.

By performing the Fourier transformation, $\hat{c}_{j,n} = 1/\sqrt{N} \sum_k e^{ink} \hat{c}_{j,k}$ with $j \in \{1, 2, \dots, J\}$ to the real space Hamiltonian (1), we can obtain the Bloch Hamiltonian $H_k = \sum_k \psi_k^\dagger h(k) \psi_k$ with $k \in [0, 2\pi]$ being the quasimomentum variable, $\psi_k = (\hat{c}_{1,k}, \hat{c}_{2,k}, \dots, \hat{c}_{J,k})^T$ and

$$h(k) = \begin{bmatrix} i\mu_1 & t_1 + \delta_1 & \dots & 0 & (t_J - \delta_J)e^{-ik} \\ t_1 - \delta_1 & i\mu_2 & \dots & 0 & 0 \\ \vdots & \vdots & \ddots & \vdots & \vdots \\ 0 & 0 & \dots & i\mu_{J-1} & t_{J-1} + \delta_{J-1} \\ (t_J + \delta_J)e^{ik} & 0 & \dots & t_{J-1} - \delta_{J-1} & i\mu_J \end{bmatrix}. \quad (2)$$

Conventionally, topological properties of 1D Hermitian systems can be characterized by the Zak phase⁷⁶, which is the Berry phase⁷⁷ associated with each band as the quasi-momentum k adiabatically runs over one cycle in the Brillouin zone. In particular, when the system consists of only two bands, the Zak phase can be obtained from the solid angle on a Bloch sphere of an eigenstate varying throughout the Brillouin zone (BZ), thus providing an intuitive geometric picture of the topology of 1D systems. In non-Hermitian systems, a pair of left and right eigenstates satisfy the biorthogonal normalization condition^{48,78}, and the non-Hermitian (always real) Zak phase can be defined as^{79,80}

$$\gamma^{(m)} = -\text{Im} \oint_{\text{BZ}} \langle \psi_{L,m}(k) | \partial_k | \psi_{R,m}(k) \rangle dk, \quad (3)$$

with $\psi_{L,m}(k)$ $\psi_{R,m}(k)$ the left (right) Bloch eigenstate and m denoting the band index. In a discrete lattice system, by considering discrete wavenumber of $k_n = 2\pi n/N_k$

and $N_k = N$ as a large integer, the Zak phase can be obtained numerically with

$$\gamma^{(m)} = -\text{Im} \sum_n^{N_k} \log[\langle \psi_{L,m}(k_n) | \psi_{R,m}(k_{n+1}) \rangle]. \quad (4)$$

However, even for a two-band non-Hermitian system, this Zak phase cannot be directly mapped onto a Bloch sphere for visualization, because the definition of left and right eigenstates leads to complex winding angles of the pseudospin vector (see Appendix A). Furthermore, as we illustrate in later discussions, non-Hermitian band structures can host topological edge states even in the presence of exceptional points. In this scenario, the Hamiltonian is not diagonalizable and the Zak phase becomes ill-defined. For these two reasons, a more versatile topological invariant is required to topologically characterize non-Hermitian multiband systems.

III. THE WINDING NUMBER OF THE MAJORANA STARS

MSR is conventionally used to represent a pure quantum high-spin state with multiple spin-1/2 states^{68–72}, and has later been extended to describe Hermitian multiband topological systems^{72–75}. For a spin- L state $|\Phi\rangle$ which has $2L+1$ components, it can be expressed in terms of $2L$ spin-1/2 states according to the Schwinger boson representation theory⁷⁰:

$$|\Phi\rangle = \frac{1}{2^{2L}} \prod_{l=1}^{2L} (\cos(\frac{\theta_l}{2}) a_{\uparrow}^{\dagger} + \sin(\frac{\theta_l}{2}) e^{i\phi_l} a_{\downarrow}^{\dagger}) |0\rangle. \quad (5)$$

Hence, a spin- L state can be decomposed to $2L$ spin-1/2 states by finding the roots of the following MSR equation⁷⁴:

$$\sum_{l=0}^{2L} \frac{(-1)^l C_{2L-l+1}}{\sqrt{(2L-l)!}} x^{2L-l} = 0, \quad (6)$$

where C_{α} denotes the wavefunction components of a spin- L state with $\alpha \in \{1, 2, \dots, 2L+1\}$, and x_l being the found MS solutions.

In non-Hermitian J-band systems, the m th right eigenstate of the system has J components in which each component can be understood as $C_{m,l}$, i.e. $|\psi_{R,m}(k)\rangle = (C_{m,1}, C_{m,2}, \dots, C_{m,J})^T$. Therefore, the m -th right eigenstate is mapped to the spin- L state by considering $2L+1 = J$. Further, the decomposition to MSRs can also be done for the right eigenstates by using the MSR equation Eq. (6), upon changing $2L$ to $J-1$ in the equation.

Since the decomposition is done for a given band m and given wavenumber k , we denote the roots of the equation to be $x_{m,l}(k) = \tan \frac{\theta_{m,l}(k)}{2} e^{i\phi_{m,l}(k)}$ with $l \in \{1, 2, \dots, J-1\}$, each representing a MS on a Bloch sphere with the spherical coordinates $(1, \theta_{m,l}(k), \phi_{m,l}(k))$. A full MSR can be obtained by tracing each MS of $x_{m,l}(k)$ on the Bloch sphere with k varying throughout the Brillouin zone.

In Hermitian systems, it has been rigorously proven that the geometrical phases of MSs, which consist of the solid angles formed by each stars and the correlation between two stars, are closely related to the Zak phases of the system^{72,73}. The existence of edge states was also known to be associated with a nontrivial winding of the system in a certain 2D plane.⁸¹ Here we define a winding number for the MSs as the total winding of their azimuthal angles. That is,

$$\nu_m = -\frac{1}{2\pi} \sum_{l=1}^{J-1} \oint \partial_k \phi_{m,l} dk, \quad (7)$$

for a given band m . In two-band systems, we have proven in Appendix A that this winding number is equivalent to the nontrivial winding of the Zak phase, which can be defined for both left and right eigenstates. However, we would like to emphasize that this winding number does not have a direct relation to the geometrical phases (which are related to solid angles instead). Still, our hope is that the winding of MSs defined for right or left eigenstates only can also be used to characterize the existence of topological edge states in multiband systems. This is confirmed by our extensive numerical results for the 1D lattice model of Eq. (1), as shown in the following sections. Of particular importance is that in non-Hermitian systems, an isolated edge state may correspond to the coalescence of multiple eigenstates. We find that the winding number thus defined summed over all energy bands satisfy the following relation:

$$\sum_m \nu_m = \sum_r D_r, \quad (8)$$

with D_r being the number of eigenstates under the open boundary condition (OBC) that coalesce into the r th isolated edge state, dubbed as a D_r -fold coalescent edge state hereafter. Note however, in a finite-size system under OBC, a D_r -fold coalescent edge state will be de-coalescent into totally D_r edge states with slightly different eigenenergies and spatial distributions, with the total number of such edge states still directly given by $\sum_m \nu_m$.

Before moving on to the next section, we stress that we have only applied the MSR to right eigenstates in the

above discussions. We have checked that using left eigenstates will yield the same conclusions.

IV. THE BULK-BOUNDARY CORRESPONDENCE

In a Hermitian 1D system, there is the bulk-boundary correspondence between the Zak phase evaluated under PBC and the number of edge states of the system under OBC^{76,82-84}. In this section, we will show that the winding number of the MSs, as defined above, can help us characterize the number of isolated edge states in non-Hermitian multiband systems, even when EPs are present in the band structure and the Zak phase is ill-defined. For the rest of this paper, we consider the model of Eq. (1) with $J = 3, 4$ as representative examples, with more demonstrations with larger J , i.e. $J = 5$, are shown in Appendix B.

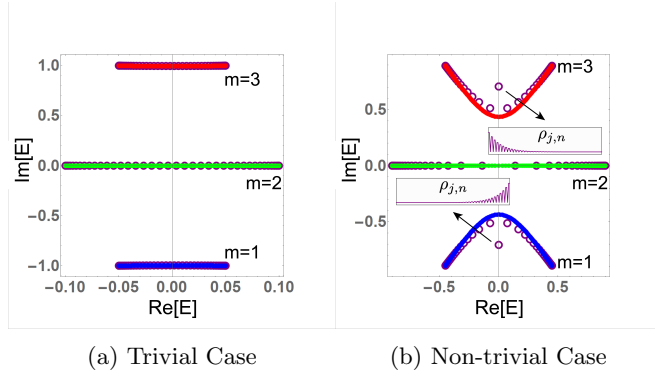


FIG. 2: (a) and (b) respectively show the energy spectra of the topologically trivial case ($t_3 = 0.1$) and non-trivial case ($t_3 = 0.9$). The purple circles indicate the energy spectrum under OBC, and the red, blue, and green curves indicate the three energy bands of the system under PBC. Parameters for both cases: $N = 120$, $t_1 = t_2 = \sqrt{2}/2$, $\mu_1 = \sqrt{2}$, $\mu_2 = 0$, $\mu_3 = -\sqrt{2}$, $\delta_j = 0$ for $j \in \{1, 2, 3\}$. Insets show the real space distributions $\rho_{j,n} = |\psi_{j,n}|^2$ of the two-fold coalescent edge states, with $\psi_{j,n}$ being the amplitude of their wavefunctions at lattice site (j, n) .

A. Reciprocal system with separable bands

We first consider a reciprocal system with $\delta_j = 0$ for $j \in \{1, 2, 3\}$, and non-Hermiticity is introduced solely from the imaginary on-site potential. In Fig. 2, we illustrate the PBC and OBC spectra for two typical cases

with and without edge states isolated from the three separable continuous bands.

In both cases, the PBC spectrum follows well with the OBC spectrum, suggesting the absence of NHSE. Thus bulk-boundary correspondence between the PBC system and isolated edge states under OBCs is expected to hold. Indeed, for the case of Fig. 2(a) without any isolated edge state, it is found that the trajectories of MSs for each band do not enclose the z -axis [Fig. 3(a)], meaning that the winding number takes $\nu_m = 0$ for $m = 1, 2, 3$. On the other hand, MSs for two of the three bands in Fig. 2(b) wind around the z -axis, indicating a nontrivial topology and corresponding edge states of the system. Note that in most cases, the trajectories of a pair of MSs for a single band exchange with each other as k varies from 0 to 2π , and go back to themselves at $k = 4\pi$. In such cases, the winding number ν_m defined as summation over all MSs for the m th band is equivalent to the total winding of one of the MSs with k varying from 0 to 4π .

In Fig. 4, we further illustrate the azimuthal angle ϕ for each MS as a function of k . We can see that for band 1 (blue) and band 3 (red) of the topologically nontrivial case, ϕ changes by 4π as k goes through the BZ twice, corresponding to winding numbers $\nu_{1,3} = 2$. On the other hand, the second band in the same case has a winding number of $\nu_2 = 0$, which is the same for any band in the topologically trivial case in Fig. 2(a). The total winding number of the nontrivial case is hence given by

$$\sum_m \nu_m = 4, \quad (9)$$

which agrees with the fact that we obtain two two-fold coalescent edge states isolated from the continuous bands in Fig. 2(b).

Finally, to understand if our proposed topological characterization at least covers the traditional Zak phase based approach, we inspect the associated Zak phases by use of Eq. (4) for a comparison. Numerically, we obtain $\gamma^{(1,2,3)} = (0.0035, -0.0035, 0)\pi$ for the topologically trivial case in Fig. 2(a), and $(0.1671, 3.8329, 0)\pi$ for the topologically nontrivial case in Fig. 2(b). Note that the Zak phases are not quantized for each individual band here, because the system we have chosen does not possess chiral symmetry nor inversion symmetry that protects a quantized Zak phase and the edge states. Nevertheless, it has been shown that in Hermitian cases, the number of edge states can be related to the summation of Zak phases of all energy bands^{83,84}. Consistent with this, we respectively obtain $\sum_m \gamma^{(m)} = 0$ and 4π for the two cases here, which are in agreement with our defined winding number and the number of two-fold coalescent edge states. This being the case, for the examples here our approach does

not outperform the Zak phase approach yet.

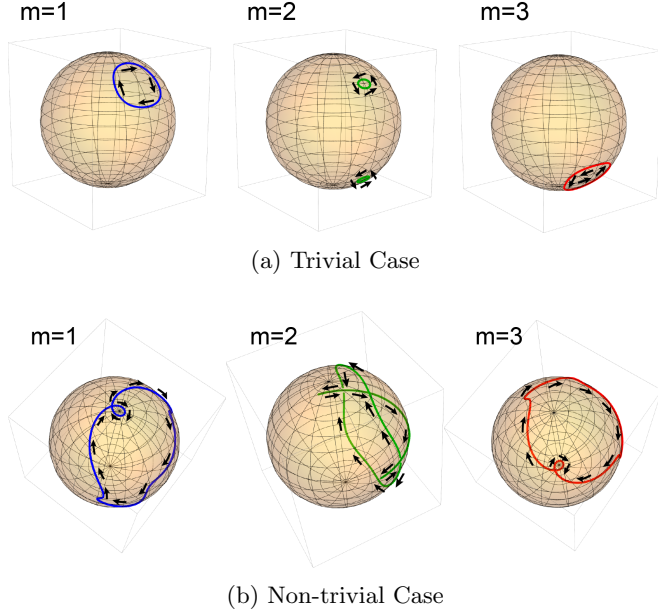


FIG. 3: Trajectories of MSs for (a) the trivial case and (b) the nontrivial case of Fig. 2. The arrows indicate the orientation of the MSs when k runs over BZ. In (a), each trajectory does not enclose the z -axis. In (b), the trajectories of MSs for the first and third bands enclose the z -axis, but those of the second band does not. Note that in most cases there is only one closed loop on the sphere, which is formed by the trajectories of two MSs of a given band connecting to each other.

B. Inseparable bands with EPs

Since the energy spectrum of a non-Hermitian system is complex in general, EPs can exist when different energy bands at the same quasi-momentum k coincide on the complex energy plane. In the presence of EPs, the eigenstates of these bands coalesce into one, leading to an incomplete Hilbert space and a non-diagonalizable Hamiltonian. Such situations are of more interest to us, because the Zak phase cannot be properly defined for each individual band. The central question is then the following: in such cases with EPs, can our defined winding numbers be used to predict the number of edge modes isolated from continuous bands on the complex energy plane?

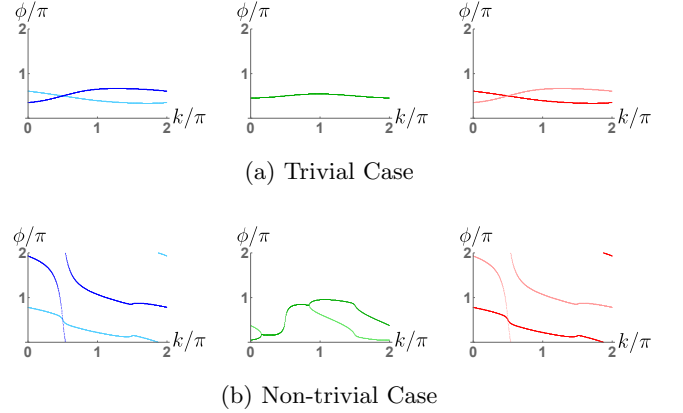


FIG. 4: (a) and (b) show the variation of angle ϕ of the MSs in the trivial and non-trivial cases respectively. In the trivial case, all three bands do not cross over 2π , hence their winding numbers are 0 according to the definition (7). In contrast, the first band (blue) and the third band (red) in the non-trivial case cross over 2π twice, indicating that they have winding numbers $\nu_m = 2$, but the winding number of the second band (green) is 0. In each panel, lighter and darker colors indicate the two MSs of each band. In most cases, each MS does not go back to itself, but connects to the other MS when k varies from 0 to 2π . The quantized winding number is thus given by the summed windings of all MSs for each band.

In Fig. 5, the three energy bands coalesce at zero energy when $k = \pm\pi/2$, and two two-fold coalescent edge states exist, well separated from the continuous bands along the imaginary axis. To see the topological origin of these coalescent edge states, we plot the three bands by three different colors in Fig. 5, and then inspect the trajectories of their associated MSs of each band in Fig. 6. It is found that the first two bands give winding numbers $\nu_m = 1$, and the third band gives $\nu_m = 2$. Collectively, the summation of the winding number agrees with the summed total number of all coalescence edge states. By contrast, the calculated Zak phase summed over all energy bands for the situation here with EPs does not give a quantized value. Clearly then, our topological characterization prevails but the Zak phase approach breaks down. As a side note, it is not always straightforward to directly observe the winding from the trajectories of MSs on the Bloch sphere, especially when the system has many bands (see Appendix B 2). Therefore, a numerical calculation through Eq. (7) should always be done to obtain the winding number.

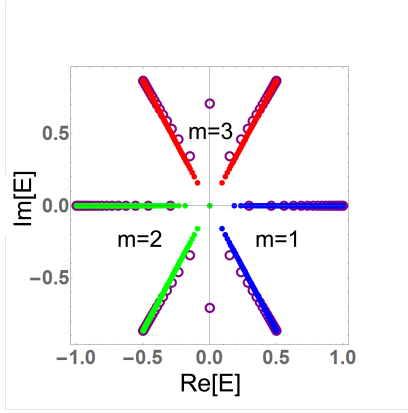


FIG. 5: Purple circles show the energy spectrum under OBC, and the red, green and blue curves show the energy spectrum of the 3 bands under PBC. All three bands coincide with each other at energy 0, causing an EP in the system. The energy gap between the EP (energy 0) and the consecutive energy is large, because the energy changes abruptly near the EP, and hence the numerical calculation cannot fully capture the continuous spectrum near the EP. Parameters are $N = 120$, $t_1 = t_2 = \sqrt{2}/2$, $t_3 = 1$, $\mu_1 = \sqrt{2}$, $\mu_2 = 0$, $\mu_3 = -\sqrt{2}$ and $\delta_j = 0$.

To further illustrate the power of our method, we provide a phase diagram by evaluating the summed winding number of MSs of the system with varying parameters $t_1 = t_2$ and t_3 , as shown in Fig. 7 with different winding numbers represented by different colors. The region where one or more EPs presents is enclosed by solid black curves, and covered by a translucent white layer on top, which are obtained from [See Appendix C]

$$\begin{aligned} 2t_1^2 + t_3^2 - 2 &= 0, \\ \sqrt{\frac{2t_1^2 + t_3^2 - 2}{3}} \frac{1}{t_1^2 t_3} &= 1, \end{aligned} \quad (10)$$

corresponding to the ellipse curve and the two almost straight lines in Fig. 7, respectively. Across these lines, the number of EPs of the continuous bands changes between zero and nonzero, representing an EP phase transition. In the absence of EP, the summed winding number agrees with the summed Zak phase (divided by π), as we have discussed in Sec. IV A. When EPs present, the Zak phase is ill-defined but we can still use the summed winding number as a topology invariant to characterize the number of isolated edge states. Note that there is a clear transition line (yellow) inside the region with the presence of EPs. Such a region with EPs is usually considered as a critical region lying between different topological phases.

Interestingly, our results indicate that within such a critical region with EPs, there is a further boundary separating different topological phases. This transition is unique in non-Hermitian systems, as edge states may be isolated from inseparable continuous bands only when they possess complex energies.

Before we proceed to the next section, we would like to strengthen that there is no gap closing along the phase transition line (yellow line). As we have briefly mentioned in Sec. IV A, the Zak phases of the bands in the system are not quantized individually, suggesting that the edge states are not protected by a band gap but only have topological origin characterized by the winding number proposed here. In fact, even in Hermitian systems it was known that topological transitions and their associated changes in edge states could occur without gap closing⁸⁵. Therefore, it is not surprising that the edge states here can emerge without the topological protection by the band gaps.

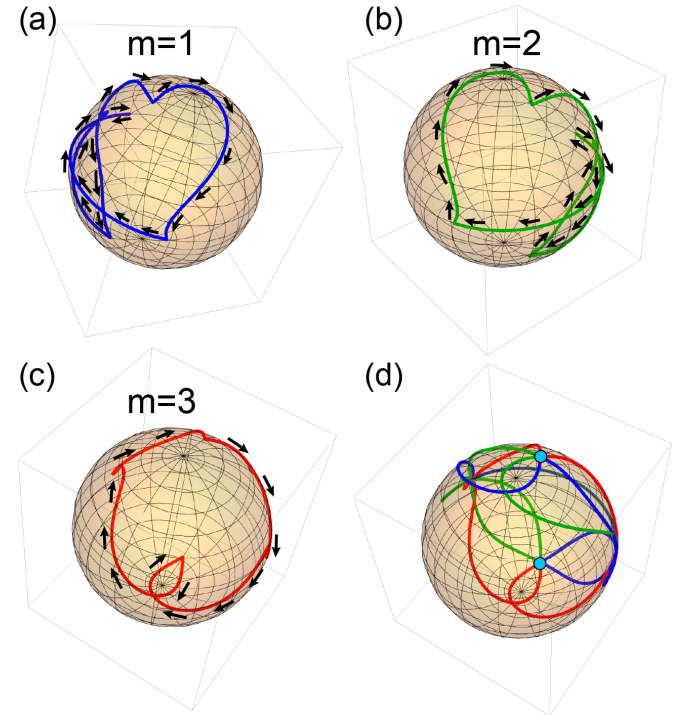


FIG. 6: (a-c) MSR for each of the three bands, corresponding to $\nu_{1,2,3} = (1, 1, 2)$ respectively. (d) the MSR of all energy bands, where two EPs are marked with light blue dots. The arrows indicate the orientation of the MSs when k runs over BZ.

C. The presence of NHSE

Although NHSE is absent in our previous examples, it plays a crucial role in many non-Hermitian systems^{38,46,49,50,52} and can greatly affect our understanding of their topological properties. With the presence of NHSE, bulk-boundary correspondence breaks down, and the energy spectrum under PBCs and OBCs behaves completely different^{46,49,54}. Therefore, we cannot directly apply the MSR method to the PBCs system and calculate the winding number to characterize isolated edge states under OBCs in this case.

To recover the bulk-boundary correspondence, we need to consider the so-called non-Bloch Hamiltonian $\tilde{h}(k) = h(k + i\kappa)$ such that for a certain κ , the energy spectrum of $\tilde{h}(k)$ does not form loops and reproduce OBC spectrum in the complex plane^{38,46,49,52,54}. Therefore, the procedure to deal with a non-Hermitian system typically consists of the following steps in general:

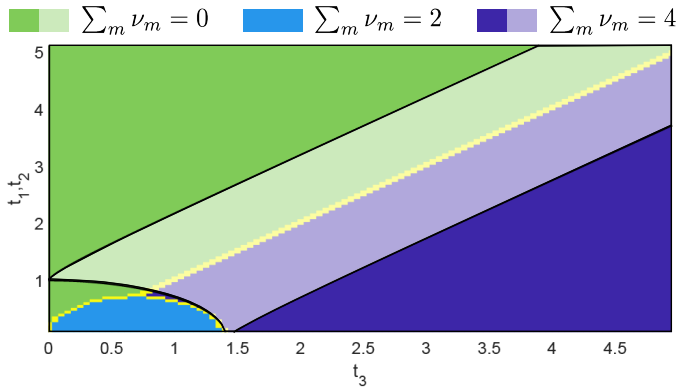


FIG. 7: The phase diagram obtained by varying the parameters $t_1 = t_2$ and t_3 . The other parameters remain unchanged, as in the previous example in Fig. 5. The winding numbers in different regions are labeled in the figure. Topological transitions occur when parameters vary across the yellow lines separating regions with different winding numbers. EP phase transitions are given by the black solid lines, and the region enclosed is covered by a translucent white layer, where the system possesses one or more EPs of continuous bands in this region.

- (i) Obtain the Bloch Hamiltonian of the system.
- (ii) Calculate the energy spectrum under both PBC and OBC.
- (iii) Check the PBC energy spectrum. If it forms loops, it means that the conventional bulk-boundary correspondence breaks down, and one needs to calculate

the GBZ described by a complex deformation of the quasimomentum $k \rightarrow k + i\kappa$ ^{46,52,61,62}. With GBZ, the non-Bloch Hamiltonian $H(k + i\kappa)$, which recovers the OBC spectrum, can be then obtained. If the PBC energy spectrum does not form any loop, it means it is free from NHSE, and we can directly proceed to the next step.

- (iv) From the non-Bloch Hamiltonian obtained, calculate the corresponding eigenstates over GBZ.
- (v) Use the MSR equation (6) to decompose the eigenstates, and then calculate the azimuthal angle of $\phi_{m,l}$.
- (vi) Calculate the winding number of MSs, which can then be used to indicate the number of isolated edge states of the system.

In Fig. 8a, we illustrate an example with the presence of both NHSE and edge states isolated from the continuous OBC band. We can evaluate the GBZ, as shown in Fig. 8c, and hence obtain the non-Bloch Hamiltonian at $\kappa \sim 2.67$ [Fig. 8b], and bulk-boundary correspondence is expected to be restored.

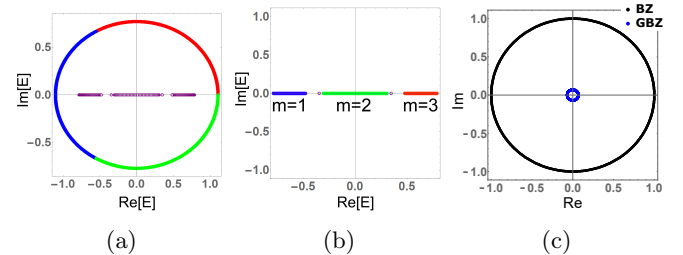


FIG. 8: (a) and (b) show the energy spectra of both PBC and OBC for the Bloch Hamiltonian and non-Bloch Hamiltonian, respectively. Purple circles indicate the energy under OBC, and the red, green and blue curves show the energy under PBC. (c) shows both the BZ and the GBZ. In (a), energy spectrum under PBC forms a loop, showing the presence of the skin effect. With GBZ, the κ can be evaluated to be 2.67, and the energy spectrum of the non-Bloch Hamiltonian under PBC recovers the OBC spectrum. Other parameters for both cases are $N = 120$, $t_1 = t_2 = 0.4$, $t_3 = 1.2$, $\delta_1 = \delta_2 = 0.2$, $\delta_3 = 1.1$ and $\mu_j = 0$.

We then calculate the MSR for the non-Bloch Hamiltonian, and the results are shown in Fig. 9. Both the summed winding number and the summed Zak phase are 4, in agreement with the fact that there are two two-fold

coalescent edge states in this case. Therefore, the bulk-boundary correspondence is fully recovered and our characterization with the winding number of the MSs remains valid for the non-Bloch Hamiltonian.

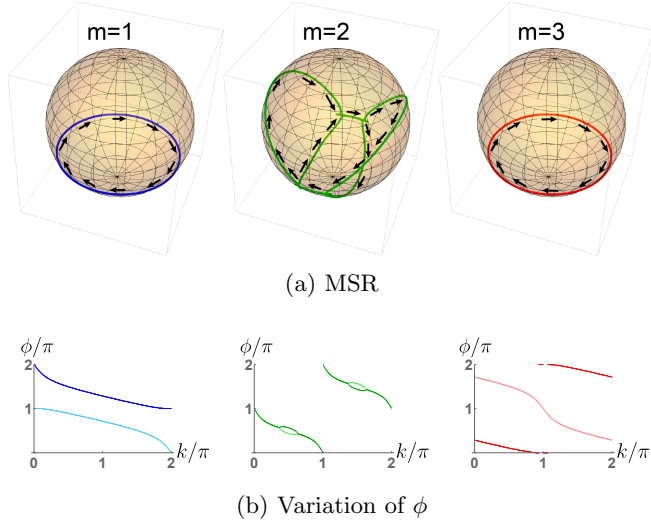


FIG. 9: The three images in (a) and (b) are corresponding to the three bands (red, blue, and green in Fig.8b respectively). The arrows indicate the orientation of the MSs when k runs over GBZ. The two colors in each plot here indicate the two MSs for a given band. Their winding number are 1, 2, 1 respectively.

D. 4-band system with 3 isolated edge states

Besides the cases with EPs, let us examine a case where the system has an odd number of isolated edge states, a situation that can never be connected with the Zak phase. In particular, we consider below a 4-band case from our model with $J = 4$, and in certain parameter regime, this case yields three non-coalescent edge states isolated from the continuous bands, as shown in Fig. 10a. NHSE also presents in this case as the PBC Bloch bands form some closed loops and are distinguished from the OBC bands. Following the procedure in Sec. IV C, we can obtain $\kappa \sim 0.75$ for the non-Bloch Hamiltonian to recover the OBC spectrum. This is illustrated in Fig. 10b.

By applying Eq. (6), we obtain the corresponding MSRs, and the obtained results are shown in Fig. 11. It is seen that the winding number is $\nu_m = 1$ for $m = 1, 2, 3$, and 0 for $m = 4$. This observation is also verified by our direct numerical approach to ν_m . Thus the summation of the winding numbers reflects the total number of isolated edge states in this case.

Remarkably, the Zak phases summed over all energy bands of non-Bloch Hamiltonian may quantize to an odd multiple of π only when the system goes around an exceptional degeneracy as we scan k from 0 to 2π , the precise situation where the system must have NHSE^{38,86}. However, by construction the NHSE has been “removed” from the non-Bloch Hamiltonian through the complex deformation $k \rightarrow k + i\kappa$. That is, the summed Zak phase can only take an even multiple of π for a non-Bloch Hamiltonian, hence cannot reflect the number of isolated edge states in this case. Indeed, numerically, we obtain $\gamma^{(1,2,3,4)} = (1.0128, 1.9608, 1.0128, 0.0136)\pi$, which sum to a quantized value of 4π , but our system has only three edge states! We have thus demonstrated again that our topological characterization is superior to the Zak phase approach.

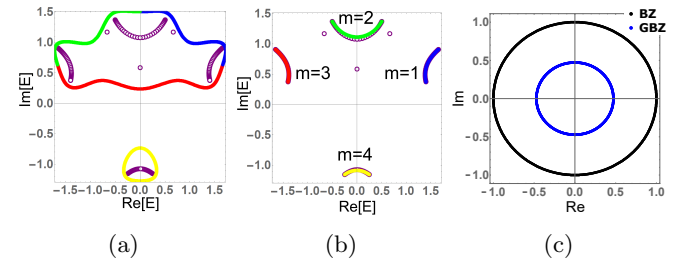


FIG. 10: (a) and (b) show the energy spectra of the Bloch Hamiltonian and non-Bloch Hamiltonian respectively. (c) shows both the BZ and the GBZ. The κ of the non-Bloch Hamiltonian is found to be 0.75. Parameters are $t_1 = 1$, $t_2 = 0.8$, $t_3 = 1$, $t_4 = 1.2$, $\delta_1 = 0.2$, $\delta_2 = 1.7$, $\delta_3 = 0.2$, $\delta_4 = 0.2$, $\mu_1 = 0.5$, $\mu_2 = -0.3$, $\mu_3 = 0.4$, $\mu_4 = 0.9$.

V. CONCLUSIONS

In summary, we have used the MSRs to decompose the eigenstates of a non-Hermitian multiband system such that we can visualize them on the Bloch sphere. We have proposed a winding number of the MSs as a new topological invariant. Our defined topological invariant successfully characterizes the number of isolated edge states of non-Hermitian multiband systems under OBC. As a marked result, our topological characterization is effective even in the presence of EPs. Indeed, the winding numbers of the MSs are more generally applicable than the Zak phase, with the latter being ill-defined as the Hamiltonian becomes non-diagonalizable. Via our proposed topological invariant, we are able to predict the change in the number of isolated edge states and hence identify topological transitions in a parameter region where EPs are present and the band are inseparable. We have further

applied our method to examples with non-Hermitian skin effects, and again verified that the bulk-boundary correspondence between the isolated edge states and the topological invariant we define can be restored by considering a non-Bloch Hamiltonian, obtained by a complex shifting of the quasi-momentum. Along this line, we have also discussed an example with an odd number of isolated edge states, where the Zak phase necessarily fails to predict the number of isolated edge states, whereas our topological invariant again agrees with the number of edge states. Such extraordinarily wide applicability of our approach may trigger further studies and bring us more insights into the interplay between exceptional degeneracies and topological properties.

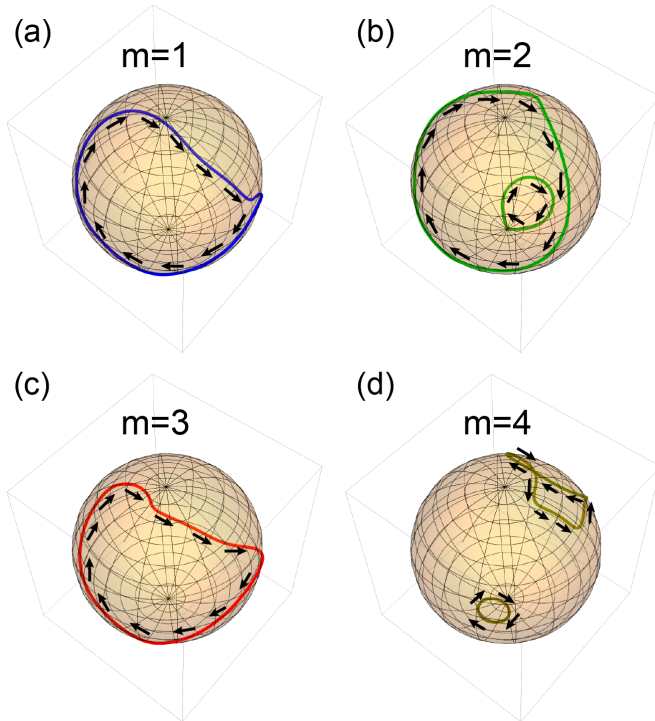


FIG. 11: The MSR of the 4 bands. (a-c) correspond to the 3 band on top in Fig.10b, and the bottom right correspond to the 1 band at the bottom in Fig.10b. The arrows indicate the orientation of the MSs when k runs over GBZ. Their winding numbers are 1,1,1,0 respectively.

Note added. During the final stage of our manuscript preparation, we became aware of a preprint⁸⁷, which uses MSRs to study a three-band non-Hermitian Lieb lattice model, with a very different focus.

ACKNOWLEDGEMENTS

J.G. acknowledges fund support by the Singapore NRF Grant No. NRF-NRFI2017-04 (WBS No. R-144-000-378-281) and by the Singapore Ministry of Education Academic Research Fund Tier-3 Grant No. MOE2017-T3-1-001 (WBS. No. R-144-000-425-592). X.Z. is supported by National Natural Science Foundation of China (Grant No. 11975166) before he joined NUS. L.L. would like to thank Chao Yang for helpful discussions.

Appendix

Appendix A: Non-Hermitian Zak phase and the winding number of the right or left eigenstates for two-band systems

A two-band non-Hermitian system can be described by the Hamiltonian

$$H = \sum_k h_x(k)\sigma_x + h_y(k)\sigma_y + h_z(k)\sigma_z + h_0(k)\mathbb{I}, \quad (\text{A1})$$

with $\sigma_{x,y,z}$ the Pauli matrices acting on a pseudospin-1/2 space, and \mathbb{I} the corresponding 2×2 identity matrix. Its left and right eigenstates are given by

$$|\psi_+^R\rangle = \begin{pmatrix} e^{-i\phi} \cos \frac{\theta}{2} \\ \sin \frac{\theta}{2} \end{pmatrix}, \quad |\psi_-^R\rangle = \begin{pmatrix} e^{-i\phi} \sin \frac{\theta}{2} \\ -\cos \frac{\theta}{2} \end{pmatrix} \quad (\text{A2})$$

and

$$\langle \psi_+^L | = \begin{pmatrix} e^{i\phi} \cos \frac{\theta}{2} \\ \sin \frac{\theta}{2} \end{pmatrix}^T, \quad \langle \psi_-^L | = \begin{pmatrix} e^{i\phi} \sin \frac{\theta}{2} \\ -\cos \frac{\theta}{2} \end{pmatrix}^T, \quad (\text{A3})$$

with $\cos \theta = h_z / \sqrt{h_x^2 + h_y^2 + h_z^2}$ and $\cos \phi = h_x / \sqrt{h_x^2 + h_y^2}$, and \pm denoting the two bands. Note that we have omitted the dependence of k for simplicity. Without loss of generality, we consider the Zak phase of the lower band, which is given by

$$\gamma^{(-)} = \text{Re} \oint_{BZ} \frac{\partial \phi}{\partial k} \sin^2 \frac{\theta}{2} dk. \quad (\text{A4})$$

In Hermitian systems with a chiral symmetry $\sigma_z h(k) \sigma_z = -h(k)$, we have $\theta = 0$, and the Zak phase is given by half of the winding angle of ϕ throughout Brillouin zone, corresponding to a quantized winding number. Degenerate topological edge states exist whenever the winding angle is nonzero. In the absence of a chiral symmetry (and other symmetries that protect 1D topology), The degeneracy of edge states will be lifted, and they are no longer protected by topology. Nevertheless, the existence of these

edge states can still be characterized by the winding number of the phase angle ϕ^{S1} , which indicates a topological origin of them despite the lack of topological protection.

For non-Hermitian systems, both angle parameters take complex values in general, thus we rewrite them as $\phi = \phi_r + i\phi_i$ and $\theta = \theta_r + i\theta_i$, with $\phi_{r,i}$ and $\theta_{r,i}$ being real. Nevertheless, due to the periodicity of the Brillouin zone, imaginary phase factors θ_i and ϕ_i must go back to their original values when k varies a period, and so does θ_r as it is originated from the altitude angle in the Hermitian limit. Therefore the winding corresponding to the Zak phase is solely given by the winding of ϕ_r .

In the main text, we have applied MSR to decompose the right eigenstates to the MSs only, containing no information of the left eigenstates. In the simplest two-band picture, each band consists of only one MS, directly given by the right eigenstates. Therefore we shall rewrite the right eigenstates with the orthogonal normalization condition, which yields

$$|\psi'_+\rangle = \begin{pmatrix} e^{-i\phi'} \cos \frac{\theta'}{2} \\ \sin \frac{\theta'}{2} \end{pmatrix}, \quad |\psi'_-\rangle = \begin{pmatrix} e^{-i\phi'} \sin \frac{\theta'}{2} \\ -\cos \frac{\theta'}{2} \end{pmatrix} \quad (\text{A5})$$

with ϕ' and θ' being real phase parameters. $|\psi'_\pm\rangle$ and $|\psi'_\pm^R\rangle$ shall be equivalent up to an overall coefficient. Taking the eigenstates of “-” band as an example, requiring $|\psi'_-\rangle = c_- |\psi_-^R\rangle$ with c_- a coefficient, it is straightforward to obtain

$$\begin{aligned} e^{-i\phi'} &= e^{-i(\phi_r + \frac{\pi}{2})} e^{\phi_i} c_- (e^{-\frac{\theta_i}{2}} e^{i\frac{\theta_r}{2}} - e^{\frac{\theta_i}{2}} e^{-i\frac{\theta_r}{2}}), \\ \cos \frac{\theta'}{2} &= \frac{c_-}{2} (e^{-\frac{\theta_i}{2}} e^{i\frac{\theta_r}{2}} + e^{\frac{\theta_i}{2}} e^{-i\frac{\theta_r}{2}}). \end{aligned} \quad (\text{A6})$$

We can see that for each individual point in the Brillouin zone, ϕ' is given by ϕ_r plus $\pi/2$ and some phases given by c_- and $\theta_{i,r}$. However, neither of these extra phases may yield a nonzero winding over a period, as c_- depends only on $\theta_{i,r}$, which must go back to themselves as discussed earlier. Therefore, with k varying from 0 to 2π , ϕ' and ϕ_r must give the same winding number, reflecting the number of isolated edge states as demonstrated in the main text. Note that we always express the decomposed MSs to be $\tan \frac{\theta}{2} e^{i\phi}$ with real phases θ and ϕ . Therefore, in the main text, we do not encounter the complex phases that we have discussed earlier in this section.

Finally, we note that though we have only considered the right eigenstates in above discussion, this analysis also applies to left eigenstates.

Appendix B: Examples in 5-band systems

MSR can also be applied to multiband systems with even more bands. Here, we provide two examples with

separable bands and inseparable bands in a 5-band system that is free from the skin effect (i.e. $\delta_j = 0$ for $j \in \{1, 2, 3, 4, 5\}$).

1. Separable bands

Considering the parameters as follow: $t_1 = t_4 = 2$, $t_2 = t_3 = \sqrt{6}/2$, $t_5 = 1.7$, $\mu_1 = -\mu_5 = 4$, $\mu_2 = -\mu_4 = 2$ and $\mu_3 = 0$. The energy spectrum is shown in Fig. 12.

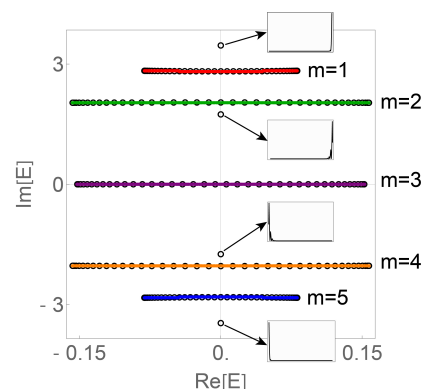


FIG. 12: Black circles show the energy spectrum under OBC, and the red, green, blue, orange and purple curves show the energy spectrum of the 5 bands under PBC. Parameters are $N = 200$, $t_1 = t_4 = 2$, $t_2 = t_3 = \sqrt{6}/2$, $t_5 = 0.9$, $\mu_1 = -\mu_5 = 4$, $\mu_2 = -\mu_4 = 2$, $\mu_3 = 0$ and $\delta_j = 0$. Insets show the real space distribution of the edge states.

Four non-coalescent edge states isolated from the continuous bands can be observed in the energy spectrum of Fig. 12. By obtaining the MSR of this model and plotting the stars on the Bloch sphere, we can also observe that the winding number is $\nu_m = 1$ for $m = 1, 2, 4, 5$ and $\nu_3 = 0$, as shown in Fig. 13.

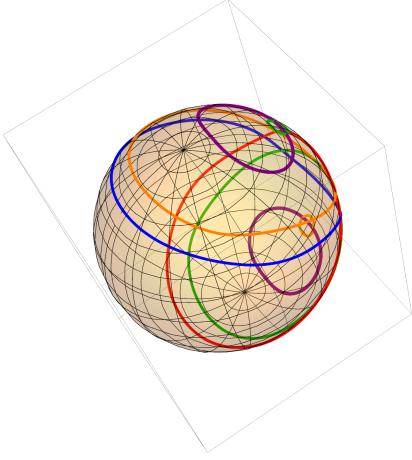


FIG. 13: The MSR of all bands are combined in the same Bloch sphere, in which the colors are corresponding to the energy bands in Fig.12

2. Inseparable bands with EPs

Considering $t_5 = 6$ and the rest of the parameters remains the same as in the previous section. The energy spectrum is shown in Fig. 14. There are also 4 isolating edge states in this case as shown in the figure. Note that the two bands with $m = 1, 2$ (blue, red) are pinned at two points on the complex energy plane, corresponding to two flat bands throughout the BZ.

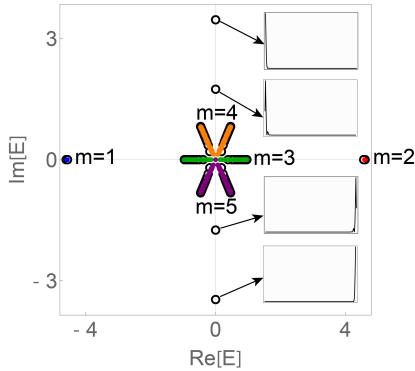


FIG. 14: Black circles show the energy spectrum under OBC, and the red, green, blue, orange and purple curves show the energy spectrum of the 5 bands under PBC. Parameters are $N = 200$, $t_1 = t_4 = 2$, $t_2 = t_3 = \sqrt{6}/2$, $t_5 = 6$, $\mu_1 = -\mu_5 = 4$, $\mu_2 = -\mu_4 = 2$, $\mu_3 = 0$ and $\delta_j = 0$. . Insets show the real space distribution of the edge states.

However, if we solve the MSR and plot it in the Bloch sphere, the stars are rather messy in this case, as shown in Fig.15. It is hard to directly obtain the winding information from the plot in higher multiband systems with the presence of EPs. Nevertheless, the winding numbers can still be obtained numerically through Eq. (7). In this specific example, the winding numbers are $\nu_m = 0$ for $m = 1, 2$, $\nu_m = 1$ for $m = 4, 5$, and $\nu_3 = 2$.

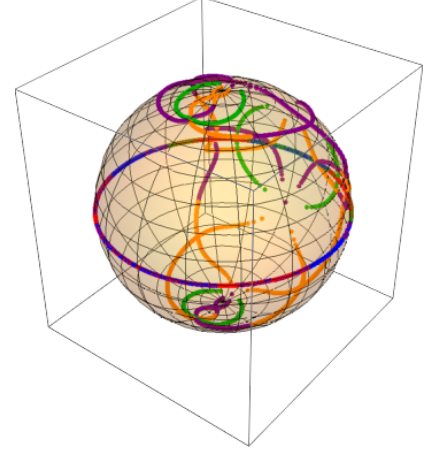


FIG. 15: The MSR of all bands are combined in the same Bloch sphere, in which the colors are corresponding to the energy bands in Fig.14.

Appendix C: solutions of EP phase boundaries

The eigenenergies of our system under PBC can be obtained from the eigenequation $\det[h(k) - E_k] = 0$ of Eq. (2) in the main text, yielding

$$E_k^3 - (2t_1^2 + t_3^2 - 2)E_k - 2t_1^2 t_3 \cos k = 0 \quad (C1)$$

for the parameters we considered in Fig. 7. In the presence of EPs, this equation can be written as $(E_k - E_1)^2(E_k - E_2) = 0$. Compared with the coefficients of Eq. (C1), we have

$$3E_1^2 = 2t_1^2 + t_3^2 - 2, \quad (C2)$$

$$E_1^3 = -t_1^2 t_3 \cos k. \quad (C3)$$

Therefore, to have a real solution of k (and hence EPs in the BZ), $-E_1^3/t_1^2 t_3$ must take a real value between -1 and 1 , and we can obtain the following two conditions:

$$2t_1^2 + t_3^2 - 2 \geq 0 \quad (C4)$$

to give a real value of E_1 , and

$$|\cos k| = \left| \sqrt{\frac{2t_1^2 + t_3^2 - 2}{3}} \frac{1}{t_1^2 t_3} \right| \leq 1. \quad (C5)$$

Thus the EP phase boundaries in Fig. 7 is obtained when the above inequalities takes the equal sign, i.e. Eqs. (10) in the main text.

-
- * phylli@nus.edu.sg
† phygj@nus.edu.sg
- ¹ Carl M. Bender and Stefan Boettcher, “Real spectra in non-hermitian hamiltonians having \mathcal{PT} symmetry,” *Phys. Rev. Lett.* **80**, 5243–5246 (1998).
 - ² Carl M Bender, “Making sense of non-hermitian hamiltonians,” *Reports on Progress in Physics* **70**, 947 (2007).
 - ³ Ingrid Rotter, “A non-hermitian hamilton operator and the physics of open quantum systems,” *Journal of Physics A: Mathematical and Theoretical* **42**, 153001 (2009).
 - ⁴ Tsuneya Yoshida, Robert Peters, and Norio Kawakami, “Non-hermitian perspective of the band structure in heavy-fermion systems,” *Physical Review B* **98**, 035141 (2018).
 - ⁵ Kazuki Yamamoto, Masaya Nakagawa, Kyosuke Adachi, Kazuaki Takasan, Masahito Ueda, and Norio Kawakami, “Theory of non-hermitian fermionic superfluidity with a complex-valued interaction,” *Physical review letters* **123**, 123601 (2019).
 - ⁶ Christian E Rüter, Konstantinos G Makris, Ramy El-Ganainy, Demetrios N Christodoulides, Mordechai Segev, and Detlef Kip, “Observation of parity-time symmetry in optics,” *Nature physics* **6**, 192–195 (2010).
 - ⁷ Stefano Longhi, “Parity-time symmetry meets photonics: A new twist in non-hermitian optics,” *EPL (Europhysics Letters)* **120**, 64001 (2018).
 - ⁸ Tomoki Ozawa, Hannah M Price, Alberto Amo, Nathan Goldman, Mohammad Hafezi, Ling Lu, Mikael C Rechtsman, David Schuster, Jonathan Simon, Oded Zilberberg, *et al.*, “Topological photonics,” *Reviews of Modern Physics* **91**, 015006 (2019).
 - ⁹ Michael V Berry, “Physics of nonhermitian degeneracies,” *Czechoslovak journal of physics* **54**, 1039–1047 (2004).
 - ¹⁰ L Jin and Z Song, “Solutions of p t-symmetric tight-binding chain and its equivalent hermitian counterpart,” *Physical Review A* **80**, 052107 (2009).
 - ¹¹ Stefano Longhi, “Pt-symmetric laser absorber,” *Physical Review A* **82**, 031801 (2010).
 - ¹² WD Heiss, “The physics of exceptional points,” *Journal of Physics A: Mathematical and Theoretical* **45**, 444016 (2012).
 - ¹³ Tony E Lee, “Anomalous edge state in a non-hermitian lattice,” *Physical review letters* **116**, 133903 (2016).
 - ¹⁴ Haitan Xu, David Mason, Luyao Jiang, and JGE Harris, “Topological energy transfer in an optomechanical system with exceptional points,” *Nature* **537**, 80 (2016).
 - ¹⁵ Absar U Hassan, Bo Zhen, Marin Soljačić, Mercedeh Khajavikhan, and Demetrios N Christodoulides, “Dynamically encircling exceptional points: exact evolution and polarization state conversion,” *Physical review letters* **118**, 093002 (2017).
 - ¹⁶ Wenchao Hu, Hailong Wang, Perry Ping Shum, and Yi Dong Chong, “Exceptional points in a non-hermitian topological pump,” *Physical Review B* **95**, 184306 (2017).
 - ¹⁷ Huitao Shen, Bo Zhen, and Liang Fu, “Topological band theory for non-hermitian hamiltonians,” *Physical review letters* **120**, 146402 (2018).
 - ¹⁸ Shubo Wang, Bo Hou, Weixin Lu, Yuntian Chen, ZQ Zhang, and CT Chan, “Arbitrary order exceptional point induced by photonic spin–orbit interaction in coupled resonators,” *Nature communications* **10**, 1–9 (2019).
 - ¹⁹ Ananya Ghatak and Tanmoy Das, “New topological invariants in non-hermitian systems,” *Journal of Physics: Condensed Matter* **31**, 263001 (2019).
 - ²⁰ Mohammad-Ali Miri and Andrea Alù, “Exceptional points in optics and photonics,” *Science* **363**, eaar7709 (2019).
 - ²¹ Xizheng Zhang and Jiangbin Gong, “Non-hermitian floquet topological phases: Exceptional points, coalescent edge modes, and the skin effect,” *Physical Review B* **101**, 045415 (2020).
 - ²² C Yuce, “Non-hermitian anomalous skin effect,” *Physics Letters A* **384**, 126094 (2020).
 - ²³ L Jin, HC Wu, Bo-Bo Wei, and Z Song, “Hybrid exceptional point created from type iii dirac point,” *arXiv preprint arXiv:1908.10512* (2019).
 - ²⁴ Yong Xu, Sheng-Tao Wang, and L-M Duan, “Weyl exceptional rings in a three-dimensional dissipative cold atomic gas,” *Physical review letters* **118**, 045701 (2017).
 - ²⁵ Johan Carlström and Emil J Bergholtz, “Exceptional links and twisted fermi ribbons in non-hermitian systems,” *Physical Review A* **98**, 042114 (2018).
 - ²⁶ Hengyun Zhou, Jong Yeon Lee, Shang Liu, and Bo Zhen, “Exceptional surfaces in pt-symmetric non-hermitian photonic systems,” *Optica* **6**, 190–193 (2019).
 - ²⁷ Kristof Moors, Alexander A Zyuzin, Alexander Yu Zyuzin, Rakesh P Tiwari, and Thomas L Schmidt, “Disorder-driven exceptional lines and fermi ribbons in tilted nodal-line semimetals,” *Physical Review B* **99**, 041116 (2019).
 - ²⁸ Huaiqiang Wang, Jiawei Ruan, and Haijun Zhang, “Non-hermitian nodal-line semimetals with an anomalous bulk-boundary correspondence,” *Physical Review B* **99**, 075130 (2019).
 - ²⁹ Zhesen Yang and Jiangping Hu, “Non-hermitian hopf-link exceptional line semimetals,” *Physical Review B* **99**, 081102 (2019).
 - ³⁰ Johan Carlström, Marcus Stålhammar, Jan Carl Budich, and Emil J Bergholtz, “Knotted non-hermitian metals,” *Physical Review B* **99**, 161115 (2019).

- ³¹ Ryo Okugawa and Takehito Yokoyama, “Topological exceptional surfaces in non-hermitian systems with parity-time and parity-particle-hole symmetries,” *Physical Review B* **99**, 041202 (2019).
- ³² Kaifa Luo, Jiajin Feng, Y. X. Zhao, and Rui Yu, “Nodal manifolds bounded by exceptional points on non-hermitian honeycomb lattices and electrical-circuit realizations,” 1810.09231v1.
- ³³ Ching Hua Lee, Guangjie Li, Yuhan Liu, Tommy Tai, Ronny Thomale, and Xiao Zhang, “Tidal surface states as fingerprints of non-hermitian nodal knot metals,” (), 1812.02011v1.
- ³⁴ Zongping Gong, Yuto Ashida, Kohei Kawabata, Kazuaki Takasan, Sho Higashikawa, and Masahito Ueda, “Topological phases of non-hermitian systems,” *Physical Review X* **8**, 031079 (2018).
- ³⁵ Chun-Hui Liu, Hui Jiang, and Shu Chen, “Topological classification of non-hermitian systems with reflection symmetry,” *Physical Review B* **99**, 125103 (2019).
- ³⁶ Kohei Kawabata, Ken Shiozaki, Masahito Ueda, and Masatoshi Sato, “Symmetry and topology in non-hermitian physics,” *Physical Review X* **9**, 041015 (2019).
- ³⁷ Hengyun Zhou and Jong Yeon Lee, “Periodic table for topological bands with non-hermitian symmetries,” *Physical Review B* **99**, 235112 (2019).
- ³⁸ Linhu Li, Ching Hua Lee, and Jiangbin Gong, “Geometric characterization of non-hermitian topological systems through the singularity ring in pseudospin vector space,” *Phys. Rev. B* **100**, 075403 (2019).
- ³⁹ Chun-Hui Liu and Shu Chen, “Topological classification of defects in non-hermitian systems,” *Physical Review B* **100**, 144106 (2019).
- ⁴⁰ Simon Lieu, “Topological symmetry classes for non-hermitian models and connections to the bosonic bogoliubov–de gennes equation,” *Physical Review B* **98**, 115135 (2018).
- ⁴¹ Kohei Kawabata, Sho Higashikawa, Zongping Gong, Yuto Ashida, and Masahito Ueda, “Topological unification of time-reversal and particle-hole symmetries in non-hermitian physics,” *Nature communications* **10**, 1–7 (2019).
- ⁴² HC Wu, L Jin, and Z Song, “Inversion symmetric non-hermitian chern insulator,” *Physical Review B* **100**, 155117 (2019).
- ⁴³ Tsuneya Yoshida, Robert Peters, Norio Kawakami, and Yasuhiro Hatsugai, “Symmetry-protected exceptional rings in two-dimensional correlated systems with chiral symmetry,” *Physical Review B* **99**, 121101 (2019).
- ⁴⁴ Tsuneya Yoshida and Yasuhiro Hatsugai, “Exceptional rings protected by emergent symmetry for mechanical systems,” *Physical Review B* **100**, 054109 (2019).
- ⁴⁵ Kohei Kawabata, Takumi Bessho, and Masatoshi Sato, “Classification of exceptional points and non-hermitian topological semimetals,” *Physical review letters* **123**, 066405 (2019).
- ⁴⁶ Shunyu Yao and Zhong Wang, “Edge states and topological invariants of non-hermitian systems,” *Physical review letters* **121**, 086803 (2018).
- ⁴⁷ Ye Xiong, “Why does bulk boundary correspondence fail in some non-hermitian topological models,” *Journal of Physics Communications* **2**, 035043 (2018).
- ⁴⁸ Flore K. Kunst, Elisabet Edvardsson, Jan Carl Budich, and Emil J. Bergholtz, “Biorthogonal bulk-boundary correspondence in non-hermitian systems,” *Phys. Rev. Lett.* **121**, 026808 (2018).
- ⁴⁹ Ching Hua Lee and Ronny Thomale, “Anatomy of skin modes and topology in non-hermitian systems,” *Physical Review B* **99**, 201103 (2019).
- ⁵⁰ Fei Song, Shunyu Yao, and Zhong Wang, “Non-hermitian topological invariants in real space,” *Phys. Rev. Lett.* **123**, 246801 (2019).
- ⁵¹ Dan S. Borgnia, Alex Jura Kruchkov, and Robert-Jan Slager, “Non-hermitian boundary modes and topology,” *Phys. Rev. Lett.* **124**, 056802 (2020).
- ⁵² Kai Zhang, Zhesen Yang, and Chen Fang, “Correspondence between winding numbers and skin modes in non-hermitian systems,” arXiv preprint arXiv:1910.01131 (2019).
- ⁵³ Tsuneya Yoshida, Tomonari Mizoguchi, and Yasuhiro Hatsugai, “Mirror skin effect and its electric circuit simulation,” 1912.12022v1.
- ⁵⁴ Ching Hua Lee, Linhu Li, Ronny Thomale, and Jiangbin Gong, “Unraveling non-hermitian pumping: emergent spectral singularities and anomalous responses,” (), 1912.06974v2.
- ⁵⁵ Stefano Longhi, “Topological phase transition in non-hermitian quasicrystals,” *Physical review letters* **122**, 237601 (2019).
- ⁵⁶ Hui Jiang, Li-Jun Lang, Chao Yang, Shi-Liang Zhu, and Shu Chen, “Interplay of non-hermitian skin effects and anderson localization in nonreciprocal quasiperiodic lattices,” *Physical Review B* **100**, 054301 (2019).
- ⁵⁷ Qi-Bo Zeng, Yan-Bin Yang, and Yong Xu, “Topological phases in non-hermitian aubry-andré-harper models,” *Physical Review B* **101**, 020201 (2020).
- ⁵⁸ Ching Hua Lee, Linhu Li, and Jiangbin Gong, “Hybrid higher-order skin-topological modes in nonreciprocal systems,” *Physical review letters* **123**, 016805 (2019).
- ⁵⁹ Linhu Li, Ching Hua Lee, and Jiangbin Gong, “Topology-induced spontaneous non-reciprocal pumping in cold-atom systems with loss,” 1910.03229v1.
- ⁶⁰ Sen Mu, Ching Hua Lee, Linhu Li, and Jiangbin Gong, “Emergent fermi surface in a many-body non-hermitian fermionic chain,” 1911.00023v1.
- ⁶¹ Kazuki Yokomizo and Shuichi Murakami, “Non-bloch band theory of non-hermitian systems,” *Physical review letters* **123**, 066404 (2019).
- ⁶² Zhesen Yang, Kai Zhang, Chen Fang, and Jiangping Hu, “Auxiliary generalized brillouin zone method in non-hermitian band theory,” (), 1912.05499v1.
- ⁶³ Nobuyuki Okuma, Kohei Kawabata, Ken Shiozaki, and Masatoshi Sato, “Topological origin of non-hermitian skin effects,” 1910.02878v3.
- ⁶⁴ X. M. Yang, P. Wang, L. Jin, and Z. Song, “Visualizing topology of real-energy gapless phase arising from excep-

- tional point,” (), 1905.07109v1.
- ⁶⁵ Chuanhao Yin, Hui Jiang, Linhu Li, Rong Lü, and Shu Chen, “Geometrical meaning of winding number and its characterization of topological phases in one-dimensional chiral non-hermitian systems,” *Physical Review A* **97**, 052115 (2018).
- ⁶⁶ Hui Jiang, Chao Yang, and Shu Chen, “Topological invariants and phase diagrams for one-dimensional two-band non-hermitian systems without chiral symmetry,” *Physical Review A* **98**, 052116 (2018).
- ⁶⁷ Hui Jiang, Rong Lü, and Shu Chen, “Topological invariants, zero mode edge states and finite size effect for a generalized non-reciprocal su-schrieffer-heeger model,” 1906.04700v1.
- ⁶⁸ Ettore Majorana, “Atomi orientati in campo magnetico variabile,” *Il Nuovo Cimento* **9**, 4350 (1932).
- ⁶⁹ F. Bloch and I. I. Rabi, “Atoms in variable magnetic fields,” *Reviews of Modern Physics* **17**, 237244 (1945).
- ⁷⁰ Lawrence C. Biedenharn and Hendrik Van Dam, *Quantum theory of angular momentum: a collection of reprints and original papers* (Academic Press, 1965).
- ⁷¹ J H Hannay, “The berry phase for spin in the majorana representation,” *Journal of Physics A: Mathematical and General* **31** (1998), 10.1088/0305-4470/31/2/002.
- ⁷² Patrick Bruno, “Quantum geometric phase in majoranas stellar representation: Mapping onto a many-body aharonov-bohm phase,” *Physical Review Letters* **108** (2012), 10.1103/physrevlett.108.240402.
- ⁷³ H.D. Liu and L.B. Fu, “Representation of berry phase by the trajectories of majorana stars,” *Physical Review Letters* **113** (2014), 10.1103/physrevlett.113.240403.
- ⁷⁴ Chao Yang, Huaiming Guo, Li-Bin Fu, and Shu Chen, “Characterization of symmetry-protected topological phases in polymerized models by trajectories of majorana stars,” *Physical Review B* **91** (2015), 10.1103/physrevb.91.125132.
- ⁷⁵ H. D. Liu and L. B. Fu, “Berry phase and quantum entanglement in majorana’s stellar representation,” *Phys. Rev. A* **94**, 022123 (2016).
- ⁷⁶ J Zak, “Berrys phase for energy bands in solids,” *Physical review letters* **62**, 2747 (1989).
- ⁷⁷ Michael Victor Berry, “Quantal phase factors accompanying adiabatic changes,” *Proceedings of the Royal Society of London. A. Mathematical and Physical Sciences* **392**, 45–57 (1984).
- ⁷⁸ Dorje C Brody, “Biorthogonal quantum mechanics,” *Journal of Physics A: Mathematical and Theoretical* **47**, 035305 (2013).
- ⁷⁹ Da-Jian Zhang, Qing-Hai Wang, and Jiangbin Gong, “Quantum geometric tensor in pt-symmetric quantum mechanics,” *Physical Review A* **99** (2019), 10.1103/physreva.99.042104.
- ⁸⁰ Da-Jian Zhang, Qing-Hai Wang, and Jiangbin Gong, “Time-dependent pt-symmetric quantum mechanics in generic non-hermitian systems,” *Physical Review A* **100** (2019), 10.1103/physreva.100.062121.
- ⁸¹ Roger SK Mong and Vasudha Shivamoggi, “Edge states and the bulk-boundary correspondence in dirac hamiltonians,” *Physical Review B* **83**, 125109 (2011).
- ⁸² Asbóth János Károly, *A Short Course on Topological Insulators: Band-structure Topology and Edge States in One and Two Dimensions* (Springer, 2016).
- ⁸³ Jun-Won Rhim, Jan Behrends, and Jens H. Bardarson, “Bulk-boundary correspondence from the intercellular zak phase,” *Phys. Rev. B* **95**, 035421 (2017).
- ⁸⁴ Han-Ting Chen, Chia-Hsun Chang, and Hsien-chung Kao, “The zak phase and winding number,” arXiv preprint arXiv:1908.06700 (2019).
- ⁸⁵ Ezawa Motohiko, Tanaka Yukio, and Nagaosa Naoto, “Topological Phase Transition without Gap Closing,” *Scientific Reports* **3**, 2790 (2013).
- ⁸⁶ Alexei A Mailybaev, Oleg N Kirillov, and Alexander P Seyranian, “Geometric phase around exceptional points,” *Physical Review A* **72**, 014104 (2005).
- ⁸⁷ Xingran Xu, Haodi Liu, Zhidong Zhang, and Zhaoxin Liang, “The non-hermitian geometrical property of 1d lieb lattice under majorana’s stellar representation,” 2002.01344v1.